A Quantitative Autoradiographic Study of the Heterogeneous Activity Distribution of Different Indium-111-Labeled Radiopharmaceuticals in Rat Tissues

Bo-Anders Jönsson, Sven-Erik Strand, and Bengt S. Larsson

Department of Radiation Physics, University of Lund and Department of Toxicology, University of Uppsala, Sweden

In light of the increased interest in small scale dosimetry, this paper presents a quantitative autoradiographic method for evaluation of heterogeneous activity distribution in tissues. This was studied in rat tissues after administration of ^{111}In-chloride, -oxine, -tropolone, ^{111}In-labeled homologous blood cells and ^{111}In-anti-CEA-F(ab')$_2$, using quantitative whole-body autoradiography. Quantification was performed utilizing an image analyzing system designed for whole-body autoradiographs. Very heterogeneous activity distribution was found in several tissues including the liver, spleen, kidneys, bone marrow, lymph nodes and testes. Notable was the high ^{111}In uptake in organs characterized as rapidly proliferating, and known to have numerous transferrin receptors. In the gastrointestinal tract, all activity was associated with the intestinal walls. The heterogeneous tissue distribution shown in this investigation accentuates the necessity for performing detailed studies of the tissue distribution of radiopharmaceuticals. This is especially important for the radiation dosimetry of radionuclides emitting beta-particles or low energy electrons. We suggest whole-body autoradiography as an excellent implement to determine local activity concentrations in organs and tissues necessary for accurate absorbed dose calculations.

J Nucl Med 1992; 33:1825–1833

Recommendations for calculating the absorbed dose to organs or tissues from radionuclides administered in the course of diagnostic medical procedures are well established (*1–3*). When these methods were formulated, the assumption was made that the radioactive substance is distributed homogeneously within the source organ. Thus, the estimation of the average absorbed dose to the entire organ is considered to be appropriately representative also in the case of individual cells in the organ. This is true for radionuclides emitting merely photons and high energy electrons, but may be fundamentally inadequate for radionuclides emitting low energy electrons. The increased interest in activity distributions at the cellular level, in both radiation protection and in radionuclide therapy, requires suitable and detailed studies of the biokinetics and the biodistribution of radionuclides and radiolabeled compounds. Whole-body autoradiography, first described by Ullberg in 1954 (*4*), is a well established and suitable technique for deriving rapid and extensive information on the detailed distribution pattern of a radioactive substance. A cautious sectioning of an animal will disclose all unexpected and expected activity sites in various organs and tissues. In order to enhance the acquired information, systems for quantification of the autoradiographs by means of digital image analyze have been developed (*5–7*).

One radionuclide of specific interest is ^{111}In because of its in vivo similarities with iron in binding to the plasma protein transferrin (*8*) and its significant accumulation in the liver, spleen and bone marrow (*9,10*). Indium-111 has a wide use in diagnostic nuclear medicine for labeling of blood cells (*11*) and monoclonal antibodies (*12–14*). In addition, ^{111}In-chloride has also been tried for the diagnosis of tumors (*15,16*) and for bone marrow scintigraphy (*17–19*). The enhanced biological effects in vivo are well established (*20,21*), and have been chased to the emission of low energy electrons (Auger and Coster-Kronig electrons) when the radionuclide is internalized by individual cells and bound in the vicinity of the DNA.

In parallel studies, we have evaluated the differences in the long-term biokinetics and biodistribution of some common ^{111}In compounds in rats after intravenous administration (*22,23*), and it has been shown that ^{111}In accumulates heterogeneously in tissues, and in or adjacent to specific cells (*24*). This investigation was undertaken to determine the macroscopic tissue distribution of some frequently used ^{111}In radiopharmaceuticals and agents used for labeling, which represent different stability properties and biokinetics (*22,23*). The study was designed to

Received Nov. 12, 1991; revision accepted Apr. 27, 1992.
For reprints contact: Bo-Anders Jönsson, PhD, Department of Radiation Physics, University of Lund, Lasarettet, S-221 85 Lund, Sweden.

quantify the activity in tissues by means of digital whole-body image analysis.

MATERIALS AND METHODS

Animals and ^{111}In Substances

Six male Wistar rats (MOELLEGAARD Breeding Centre, Denmark) were intravenously injected with one of the following substances: ^{111}In-chloride, ^{111}In-TRIS-8-hydroxyquinoline (oxine), ^{111}In-2-hydroxy-2,4,6-cycloheptatrenine (tropolone), ^{111}In-oxine-labeled platelets or mixed leukocytes, and finally an ^{111}In-anti-CEA-F(ab')$_2$, BW431/31, (Scintimun®, Behringwerke, Marburg, Germany). Injected ^{111}In activities were 18 MBq for ^{111}In-chloride, ^{111}In-oxine and ^{111}In-tropolone, 10 MBq for ^{111}In-oxine labeled homologous blood cells, and 25 MBq for ^{111}In-anti-CEA-F(ab')$_2$. The labeling procedures for the platelets and leukocytes were slight modifications of established methods (*25,26*), and the labeling efficiency was 76% and 59%, respectively. The rats, weighing approximately 240 g, were maintained on a standard laboratory diet and water ad libitum in separate cages and were killed 5 days after the injection by inhalation of carbon dioxide. The activities in the animals at this time were 2–3 MBq.

Whole-Body Autoradiography Characteristics of ^{111}In

Indium-111 decays by electron capture with a half-life of 2.83 days (*27*). The mono-energetic conversion electrons from ^{111}In provide suitable characteristics for autoradiography (Table 1). For a pre-exposure film experiment, a fine-grained x-ray film (Structurix D7, Agfa-Geavert, Germany) was chosen for high resolution in the autoradiographs. Film sheets were exposed from 20, 60 and 80 μm thick sections from a pilot rat injected with ^{111}In-oxine and prepared as described below.

Preparation of Whole-Body Sections

The method used for whole-body autoradiography has been reviewed in detail elsewhere (*28,29*). Briefly, the dead animal was immersed in a −70°C mixture of liquid hexane and solid carbon dioxide for 5 min, and then transferred to a cold room at −20°C. This was repeated for all the animals before the actual embedding. The frozen animal was then accurately positioned horizontally on a cryo-microtome stage surrounded by a metal frame, refrozen in hexane into a block of carboxymethyl cellulose (CMC) gel for 1 hr and stored in the cold room until it reached the equilibrium temperature (−20°C). Approximately 25 sagittal sections at various levels, both 20 and 60 μm thick, were cut from all animals with a cryo-microtome (LKB 2250). The sections were picked up on an adhesive tape (Scotch 3M no. 810). The sections were freeze-dried at −20°C and then attached to x-ray film and put into cassettes. After an appropriate exposure time, the film and section were separated and the film was developed (Kodak D-19) and fixed (Kodak F-24).

TABLE 1
Summary of Emitted Radiation During the Decay of ^{111}In*

Radiations	Average energy (keV)	Yield (Bq s^{-1})	Range† (μm)
Photons			
γ_1	171.3	0.905	
γ_2	245.3	0.940	
K_α, x-rays	23.1	0.680	
K_β, x-rays	26.2	0.146	
Conversion electrons	144.6	0.0841	194
	168.0	0.0130	254
	218.6	0.0503	386
	242.1	0.0097	445

* Auger electrons omitted. For the complete decay, see (27).

† Ranges are x_{90}-values, i.e., the radius of a sphere in which 90% of the electron energy is absorbed (2).

Image Analysis Procedure

A computerized image analyzing system specifically adapted for whole-body autoradiography was used for the quantification of the autoradiographs and has been described in detail elsewhere (*7,30*). Briefly, the image sampling device is a video camera (Philips LDH 400/61) in an adjustable position above a light box (Novalux A4E, Photron, Sweden). The video signal is transferred to a microcomputer (Cromemco System 2-HD) via an image digitizer (384 × 241 pixels and 256 grey levels). Using a digitizer pad, regions of interest (ROIs) can be indicated on a stored image, and the grey level distribution is displayed as a pixel histogram (y-axis) as a function of the grey levels (x-axis). By using different selected "windows" of the histograms, it is possible to scan the grey level distribution and get detailed information about the location, mean optical density, standard deviation of the optical density and the number of pixels within the selected window. The corresponding area is displayed in color on the original image.

Calibration for Optical Density Measurement

To allow accurate measurements of the optical density over the autoradiographs, a careful calibration of the image processing system was performed before the analysis. A series of grey filters representing known optical densities, including 0.10, 0.30, 0.50, 0.70 and 1.00 (Kodak Wratten gelatin filter no. 96, Eastman Kodak Comp., Rochester, NY), was used to calibrate the grey levels so that they matched the optical density. This procedure was performed following a special calibration software routine allowing for precise density measurements (*7,30*). Images of the grey filters were sampled and the digitized images were divided into several square subfields, from which locally adjusted calibration curves were calculated to give the true density for subsequent measurements. A precision of within ± 0.01 density unit is possible to obtain.

Activity Standards

Optical density can be correlated to activity concentration if a standard radionuclide staircase of several known activity concentrations is used to expose a reference film. A liver homogenate was prepared from a fresh rat liver using a Potten-Elvejham homogenizer. Aliquots of the homogenate were divided between small plastic Ellermann-tubes, and accurately pre-calibrated ^{111}In-oxine activities were added. The samples were allowed to incubate for 30 min. The cell homogenates were then stored in a cooler. A CMC-block was prepared by filling a microtome-stage form, which was then frozen in hexane. In the cold room, holes, 6.3 mm in diameter, were drilled in the CMC-block to form small wells. The homogenates, including one without activity, were vortexed and centrifuged to remove air bubbles and put into the wells with syringes. The block was then carefully refrozen. The same procedure as above was performed for ^{111}In-labeled whole blood. The ^{111}In staircase was cut in the same manner as the animals in 20, 60 and 80 μm thicknesses and put on film at the

same time and with the same exposure time. After exposure, the activity standards were measured for activity with a high-purity germanium detector, HPGe (Canberra). Activity standards were also made directly from animal sections.

Analysis and Quantification of Autoradiographs

The mean optical densities of the various autoradiographs of the ^{111}In staircase were determined as above, and the corresponding cumulated activities per area unit and per mass unit were calculated. The cumulated activity, $\tilde{A}$, is the time-integrated decays during the time of exposure, i.e., the number of disintegrations in the source of interest during exposure of the film:

$$\tilde{A}(t_1, t_2) = A_0 \int_{t_1}^{t_2} e^{-\lambda t} dt = \frac{A_0}{\lambda}[e^{-\lambda t_1} - e^{-\lambda t_2}], \qquad \text{Eq. 1}$$

where $\tilde{A}$ (t_1, t_2) is the number of disintegrations between t_1 and t_2 (Bq h), A_0 is the activity at start of exposure (Bq) and λ is the physical decay constant (s^{-1}).

The spatial resolution of the autoradiographs was analyzed by placing a digital profile across an ^{111}In standard autoradiograph and examining the density profile, i.e., the distribution of silver grains from the edge of the source and outward (Fig. 1). The distance from the edge to the point where the optical density has decreased to half was defined as the spatial resolution.

All animal autoradiographs were examined qualitatively, and selected autoradiographs were analyzed quantitatively. ROIs were drawn on interesting tissues and organ parts and the corresponding grey level histogram, now given as the number of pixels with a specific optical density, was examined in detail. Normally four different sagittal levels of a selected organ or tissue part were analyzed digitally for activity concentration and the degree of heterogeneity.

RESULTS

Activity Calibration

The pre-exposure film test showed that for the activities chosen two weeks of exposure was well suited to the activity concentrations in the tissue sections, with no parts of a section being overexposed. Control exposure from sections without activity did not result in any blackening of the film. The spatial resolution, analyzed from a digital profile across an ^{111}In standard autoradiograph, was estimated to be approximately 100 μm for 20 μm thick sections (Fig. 1). For both 60 and 80 μm thick sections, the resolution was determined to be approximately 150 μm.

The calibration of the film using ^{111}In-oxine-labeled blood and liver homogenate sources resulted in curves of similar characteristics. Figure 2 shows the optical density as a function of the log exposure, given as the cumulated activity, $\tilde{A}$, (kBq h) per mass unit, m, (mg). The maximum slope of the curve is almost the same for the 60 and 80 μm sections, whereas 20 μm sections seem to underexpose the film for small cumulated activities, <10 kBq h mg^{-1}, thus resulting in poorer image contrast. Although we failed to reach the "knee" of the curves, which should be just above 1.0, the range suitable for autoradiography appears to be 0.1–1.0 optical density, where the best image contrast will be obtained. Activity standards made directly from animal sections supported the optical density results obtained from the ^{111}In staircase (results not shown). The absorption of radiation within the sections is also illustrated in Figure 2, in which the distance between the curves is decreased if the corresponding thickness of the sections is increased. A standard curve may be established as a log-log relationship between optical density (OD) and the exposure, i.e., cumulated activity per mass unit (kBq h mg^{-1}) (Fig. 3). The expression for the linear portion of the curve can be written as:

$$\log(\mathrm{OD}) = k \cdot \log\left(\frac{\tilde{A}}{m}\right) + l, \qquad \text{Eq. 2}$$

where l is the y-axis intercept and k is the slope of the curve. A computer-generated linear regression of the

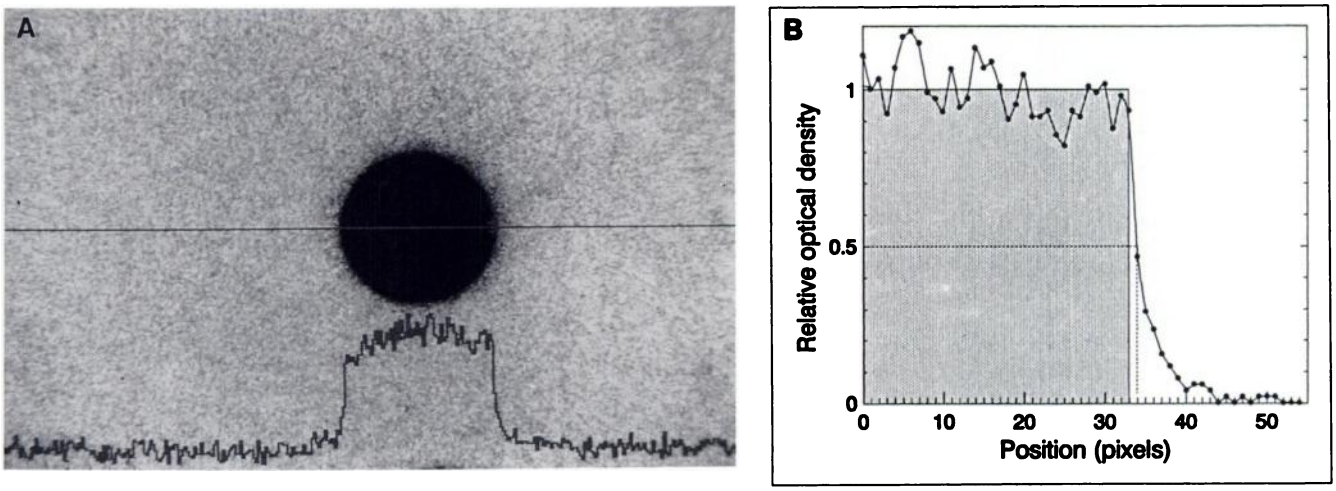

FIGURE 1. Graph of the relative optical density demonstrating the edge-spread function obtained from one of the 20 μm activity standards. A digital profile was layed across the autoradiograph (A) to measure the spatial resolution, which may be defined as the half density distance. The spatial resolution was found to be approximately 100 μm and 150 μm for 20 (B) and 60 μm sections, respectively, where 100 μm approximately corresponds to a 1-pixel length.

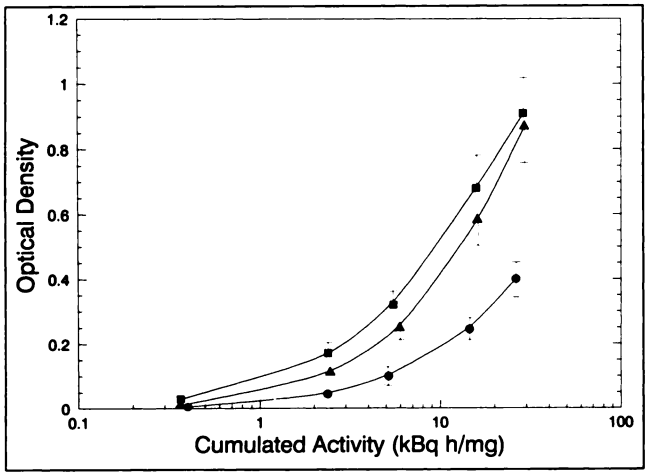

FIGURE 2. Response curves showing the optical density (OD) as a function of log exposure, i.e. cumulated activity per unit mass, for a section thickness of 20 μm (circles), 60 μm (triangles) and 80 μm (squares). Each data point is the mean of three measurements, and the uncertainty is given as the standard deviation of the OD calculated by the software.

curves gives the "density-activity" relationships which were used in the analysis of all rat autoradiographs (Table 2). These equations may then be used for ^{111}In sections exposing the Structurix film used, regardless of the time of exposure. To obtain the activity content (kBq mg^{-1}) in a tissue section, the cumulated activity is simply divided by the number of disintegrations during the exposure, i.e., the time-integrated decays.

Activity Distribution in Whole-Body Autoradiography

The patterns of the activity distribution were found to be almost the same, regardless of the radiopharmaceutical injected (Fig. 4). After intravenous injection of ^{111}In-chloride, ^{111}In-oxine or ^{111}In-tropolone, the activity was highly concentrated in fast dividing tissues, such as the bone marrow, bowel walls, testes, skin and the pulp cavity of the incisor teeth. High concentrations of activity were also found in the liver, spleen, kidneys and lymph nodes, whereas medium activity contents were found in the muscles, lungs and cardiac muscle. No blackening at all could be seen over the brain, skeletal bone or in the intestinal contents. One major difference between the substances was the rate of blood elimination, which has been found to be delayed after injection of ^{111}In-oxine (*22*). This is because ^{111}In-oxine very rapidly labels circulating erythrocytes, resulting in a longer retention time. For the other substances, blood elimination was faster and no activity can be seen in the blood on Day 5 in the case of chloride and F(ab')$_2$, while only a minor fraction is seen in the case of tropolone (compare the heart chambers in Fig. 4, panels A, C, D and E).

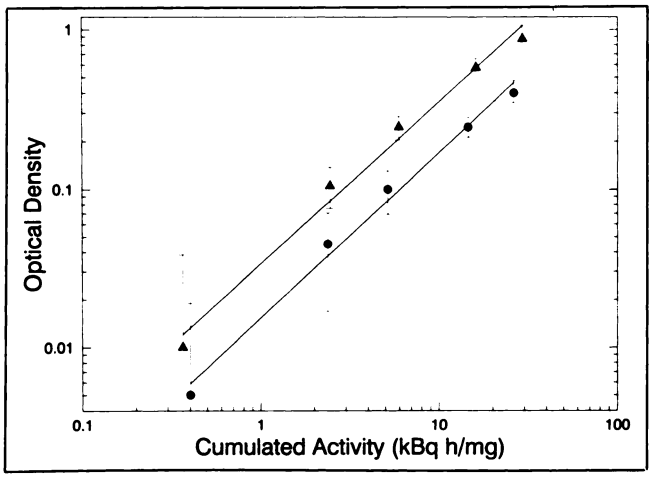

FIGURE 3. Standard curve presented as a log-log plot of log (OD) versus log (Ã/m) of ^{111}In liver standards. Section thicknesses are 20 μm (circles) and 60 μm (triangles). The expression for the linear part of the curve can be represented as log(OD) = k · log(Ã/m) + l, which was used for transposing optical density measurements to cumulated activity.

TABLE 2
Relationship Between Optical Density (OD) and Cumulated Activity Estimated from Data in Figure 3*

Equation: Y = kX + l	r^2
20 μm: log(OD) = (1.05 ± 0.06)·log(Ã/m) − (1.79 ± 0.08)	0.99
60 μm: log(OD) = (1.02 ± 0.06)·log(Ã/m) − (1.45 ± 0.09)	0.98

* The uncertainty values are the estimated standard error of declination coefficient and y value, respectively.

A marked heterogeneous distribution of ^{111}In activity was found in some organs, such as the liver, spleen, kidney, lymph nodes and testes. Figure 5 shows magnifications of parts of the whole-body autoradiographs. The activity in those organs accumulated in a complex pattern showing discrete histologic parts. In the spleen (Fig. 5A), the activity was mainly localized in the red pulp, and in the kidney (Fig. 5B) a markedly heterogeneous activity accumulation can be observed in the cortex, whereas the medulla shows only slight uptake. A noticeably grainy pattern is evident in the liver (Fig. 5C) where the activity localized mainly to specific regions. The white areas in the liver indicate activity-free blood vessels. Note in the same image that in the gastrointestinal system the activity is associated only with the walls. In the bone marrow (Fig. 5D), as well as in the lymph nodes (Fig. 5E) several hot spots were found. The skeleton also seen in Figure 5D shows almost no activity. The testes (Fig. 5F) finally show a complex activity pattern that is probably associated with the tubules of the testes.

Quantification of Whole-Body Autoradiography

The autoradiographic results are consistent with previous biodistribution studies of the same substances (*22, 23*), and activity concentrations are of the same magnitude. In Table 3, the uptake values estimated from the autoradiographs using the calibration in Figure 3 are given

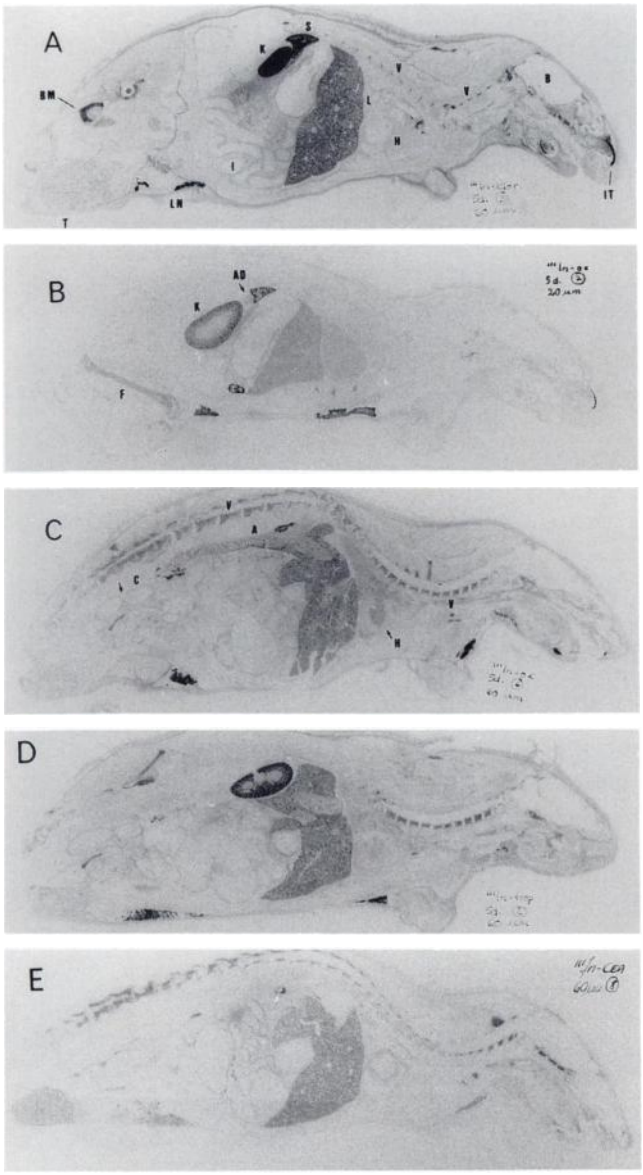

FIGURE 4. Autoradiographs of whole-body sections from rats 5 days after injection of: (A) ^{111}In-chloride, (B–C) ^{111}In-oxine, (D) ^{111}In-tropolone and (E) ^{111}In-anti-CEA-F(ab′)$_2$. The dark areas indicate the presence of activity and show that several tissues have accumulated a significant amount of ^{111}In. Note that several organs and tissues that have taken up activity are characterized as fast proliferating, e.g., bone marrow, testes, intestinal walls, skin and the pulp cavity of the incisor teeth. BM = bone marrow; I = intestines; K = kidneys; S = spleen; L = lungs; H = heart; LN = lymph nodes; V = vertebrae; B = brain; IT = inscisor teeth; F = femur; A = aorta; AD = adrenals; C = colon (note the constriction for the formation of stool, arrow in panel C). In the case of ^{111}In-oxine, the higher blood activity compared with the other radiopharmaceuticals is clearly shown.

as the % g^{-1} tissue per injected activity and are corrected for physical decay to the time of administration.

The ^{111}In distribution in organs and parts of organs was measured as the mean optical density. This should correspond to a criterion of the mean absorbed dose to the organ if the activity were uniformly distributed throughout the whole organ and a proportional relationship were valid. The activity distribution was, however, highly heterogeneous in several organs. This heterogeneity was evaluated in the ROI for each tissue as the percentage of pixels in that tissue area above or below the average optical density (corresponding to the average activity after calibration) in the organ section. Values for liver, spleen, bone marrow and inguinal lymph nodes are presented in Table 4. The values are ratios, given in intervals of 0.25, and are the mean of three to four autoradiographic section levels. It can be seen that most of the pixels correspond to an optical density adjacent to the average optical density. For some substances and tissues, however, a relatively large fraction of the drawn ROI deviates considerably from the average optical density. Among several organs in which the heterogeneous activity distribution is easily discernible, are the spleen and the kidney (Fig. 5A–B). In these two organs, all ^{111}In substances studied accumulated significantly in discrete structures. For chloride, oxine and tropolone, the ^{111}In activity was on the average trapped by 69% ± 9% (1 s.d., n = 17) of the spleen volume (estimated from the autoradiographic area) identified as the red pulp. The white pulp (31% ± 9%) was without activity. For anti-CEA-F(ab′)$_2$, 56% of the spleen was labeled, while the value for ^{111}In-leukocytes was 80%. In the kidney, the cortex accumulated most of the ^{111}In activity (Fig. 5B). Scanned pixel-histograms for chloride, oxine, tropolone and anti-CEA-F(ab′)$_2$ were converted to the percentage of the tissue area with a specific optical density relative to the optical density averaged over the whole ROI and are presented as bar diagrams in Figure 6. In the case of CEA-F(ab′)$_2$, it can be seen that the ratio between the hot spots in the cortex and the cold area in the medulla is close to a factor 10.

DISCUSSION

Previous studies have indicated substantial ^{111}In accumulation with long retention times in several tissues after administration of ^{111}In-labeled substances (*22,23*). In this investigation, a noticeable heterogeneous distribution of ^{111}In was found in both expected and unexpected tissues of the rat body. The pattern was almost the same, regardless of which ^{111}In radiopharmaceutical was administered. The activity accumulated strongly in fast dividing tissues, like the bone marrow, intestinal walls, testes, skin and the pulp cavity of the incisor teeth. High concentrations of activity were also found in the liver, spleen, kidneys and lymph nodes. Many physiologic and biochemical factors influence the in vivo localization and retention of a radiolabeled compound. The elimination of ^{111}In from several tissues is prolonged, which indicates an almost irreversible labeling to organ cells. It has been shown that ionic indium, like iron and gallium isotopes, is trapped by transferrin in the plasma (*8,31*) and forms a stable indium-transferrin complex. In the course of time, transchelation to transferrin from different radiochelates (*32*) and antibodies (*33*)

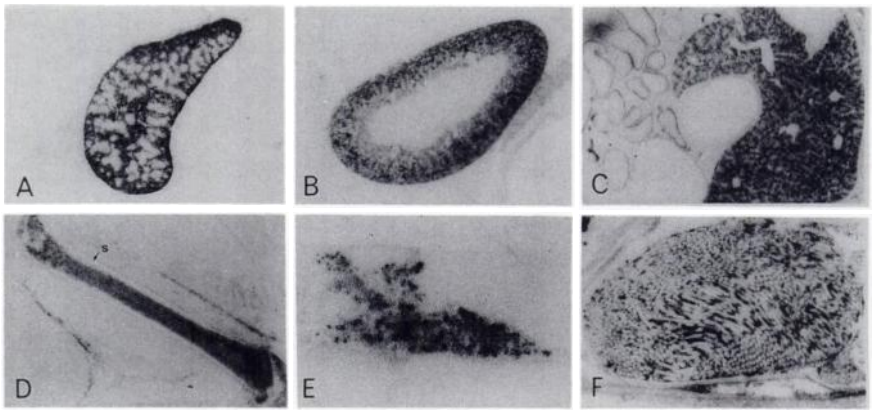

FIGURE 5. Detailed parts from whole-body autoradiographs showing markedly heterogeneous activity distribution. (A) Spleen, (B) Kidney, (C) Liver and intestinal walls, (D) Bone marrow in femur (s = skeleton bone), (E) inguinal lymph nodes and (F) testes. See Tables 3 and 4 for quantitative information.

takes place in vivo. It is likely that ^{111}In-transferrin identifies cells expressing transferrin receptors (*34,35*) and it is possible that ^{111}In-transferrin is taken up by receptor-mediated endocytosis (*36,37*). This assumption is supported quite well by the significant accumulation in fast dividing tissues, the cells of which express a large number of transferrin receptors (*38*), thus making them potential targets for ^{111}In-transferrin.

The results in the present study represent situations in which calculation of the absorbed dose based on recommended methods may underestimate the absorbed dose to fractions of cell clusters or single cells in a specific organ because of a heterogeneous activity distribution. This is especially the case in situations where radionuclides emitting low energy electrons are internalized into the cytoplasm and nucleus of a cell. This is particularly serious if the cells for which the absorbed doses are underestimated are radiosensitive cells, such as hematopoetic stem cells in the red bone marrow or germ cells in the reproductive system. At the same time, however, the absorbed dose to cells in activity-free regions will be overestimated, which is obvious in the white pulp of the spleen or the kidney medulla in this study. Other tissues of special interest are the lymphatics. It was found that a significant accumulation took place in different lymphatic organs, i.e., the lymph nodes, spleen and cecum. The lymph nodes and the spleen are of special radiobiological interest and the former are not currently considered in absorbed dose estimations (*3*).

The ^{111}In distribution in organs and parts of organs was measured as the mean optical density. As shown above, it is possible to transform the measured optical density to cumulated activity (kBq h) per unit area or per unit mass. The activity concentration for specific regions may then be calculated and used as basic data for the calculation of macroscopic absorbed doses to, for example, large cell

TABLE 3
Activity (% g^{-1}) in Organ Sections at the Time Animals Were Killed*

Organ	^{111}In-labeled compound					
	Chloride	Oxine	Tropolone	F(ab')$_2$	Leukocytes	Platelets
Liver	1.6† (1.2–2.3)‡	2.7 (2.0–3.6)	1.5 (1.1–2.1)	1.0 (0.8–1.5)	2.6 (2.0–3.4)	2.8 (2.3–3.7)
Spleen	3.6 (2.5–5.5)	4.2 (3.1–5.8)	4.3 (3.2–6.0)	3.6 (2.8–5.0)	19.6 (14.0–28.7)	34.6 (24.2–51.4)
Bone marrow	1.9 (1.4–2.8)	1.6 (1.2–2.1)	2.0 (1.5–2.8)	1.1 (0.9–1.5)	—	2.3 (1.9–2.9)
Lymph nodes	2.6 (1.9–3.8)	4.4 (3.2–6.2)	3.1 (2.3–4.4)	0.7 (0.5–0.9)	—	—
Kidneys	3.8 (2.6–5.5)	3.5 (2.6–4.8)	3.2 (2.4–4.5)	8.9 (6.3–13.1)	—	—
Testes	0.5 (0.4–0.6)	0.5 (0.4–0.7)	0.7 (0.5–0.9)	0.7 (0.5–0.8)	—	—
Intestinal wall	0.8 (0.6–1.2)	2.0 (1.6–2.7)	1.3 (1.0–1.7)	0.7 (0.5–0.9)	—	—

* Values corrected for physical decay.
† Mean of four analyses at different section levels.
‡ Figures in parentheses are the lowest and highest value with respect to the uncertainties (estimated standard errors) in the relationships in Table 2.

TABLE 4
Percentage of Pixels in a Tissue Area (a Drawn ROI) Above or Below the Average Optical Density (Corresponding to the Average Activity After Calibration) in the Organ Section

	% ROI Interval					
Tissue/Substance	<0.5	0.5–0.75	0.75–1.0	1.0–1.25	1.25–1.50	>1.5
Liver						
^{111}In-chloride	—	3.2	43.8	40.2	12.8	—
^{111}In-In-oxine	4.4	—	40.3	47.0	8.3	—
^{111}In-tropolone	2.8	15.6	32.0	33.0	14.5	2.1
^{111}In-F(ab')$_2$	8.8	—	44.6	36.8	7.6	2.2
^{111}In-leukocytes	12.0	—	53.3	—	32.6	2.1
^{111}In-platelets	20.2	—	22.0	35.4	—	22.8
Spleen						
^{111}In-chloride	—	23.4	27.8	34.3	14.5	—
^{111}In-oxine	3.1	10.1	33.8	25.8	24.8	2.4
^{111}In-tropolone	1.4	8.5	37.9	28.6	23.6	—
^{111}In-F(ab')$_2$	8.3	16.2	28.0	22.2	15.3	10.0
^{111}In-leukocytes	3.6	19.4	23.9	27.3	20.6	5.2
^{111}In-platelets	6.4	12.4	21.3	34.6	22.8	2.5
Bone marrow						
^{111}In-chloride	—	18.4	38.8	28.6	11.7	3.3
^{111}In-oxine	3.1	24.2	26.7	31.9	11.8	2.3
^{111}In-tropolone	—	33.7	29.5	22.0	11.7	3.1
^{111}In-F(ab')$_2$	3.7	21.7	20.0	31.7	20.5	2.4
^{111}In-platelets	24.4	—	29.0	30.8	—	15.8
Lymph nodes						
^{111}In-chloride	21.0	13.6	15.1	18.5	20.3	11.5
^{111}In-oxine	2.8	7.0	42.4	22.3	20.3	5.2
^{111}In-tropolone	8.7	21.6	17.0	23.6	17.7	11.4
^{111}In-F(ab')$_2$	2.1	29.6	49.0	18.2	—	1.1

Uncertainty in values is approximately ± 20%.
Values are given ratios in intervals of 0.25, and are the mean of three to four autoradiographic section levels.

clusters with an appropriate cell-to-cell calculations method (*39,40*). The increased interest in activity distributions at the cellular level, in both radiation protection research and in radionuclide therapy, requires suitable techniques for such studies. Experimental efforts have been made to evaluate three-dimensional dosimetry (*41,42*) and combine quantitative autoradiography with in vivo microthermoluminescence dosimeter measurements for radioimmunotherapy (*43,44*). Estimations of the energy imparted to individual cells that have accumulated activity can be made, however, only from micro-autoradiographic experiments showing exact localization. The purpose of

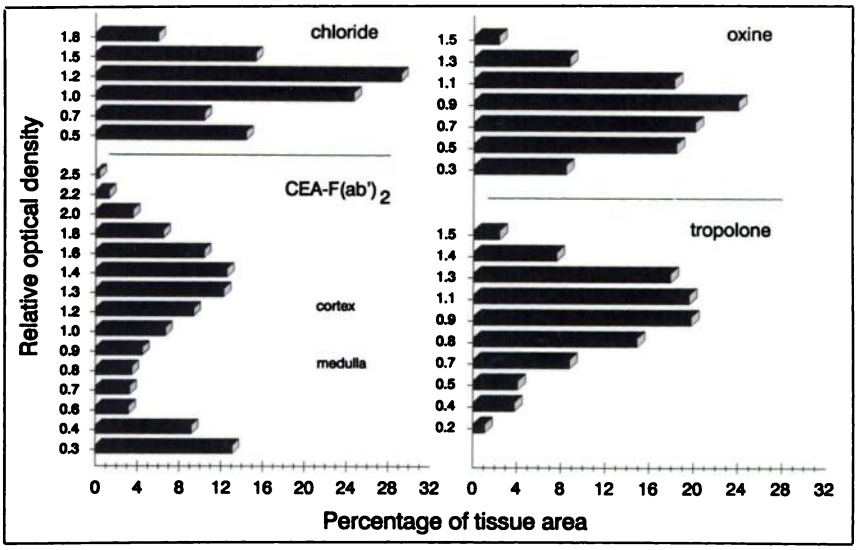

FIGURE 6. The activity distribution in the kidneys after administration of ^{111}In-radiopharmaceuticals (chloride, oxine, tropolone, and CEA-F(ab')$_2$). The bars represent the percentage of tissue area with a specific optical density (or activity) relative to the optical density (or activity) averaged over the whole tissue area (i.e., a drawn ROI). It can be seen that the ratio between *hot spots* in the cortex and the *cold* area in the medulla varies from a factor of 5 to more than 8.

this study was to make a detailed investigation of the whole-body distribution of some common ^{111}In compounds using quantitative autoradiography, while especially concentrating on estimating the magnitude of the heterogeneously distributed activity in different tissues. In forthcoming papers (*45,46*), we confirmed and qualitatively determined the cellular and subcellular localization of indium in testes and red bone marrow cells.

In conclusion, quantitative macro-autoradiography offers a technique that makes it possible to study the non-uniform distribution of a radioactive compound in tissues and to estimate its activity concentration in detail. We have shown that ^{111}In accumulation is markedly heterogeneous in numerous organs and tissues, particularly in rapidly proliferating tissues. Studies of cellular and subcellular localization of indium and other radionuclides in those tissues should be of great value for the future of this new approach to radiation protection.

ACKNOWLEDGMENTS

The authors thank Ms. Eva Carlsson at the Department of Radiation Physics, Lund, for technical assistance and Mr. Daniel Lareya, Department of Toxicology, Biomedical Center, Uppsala. This investigation was supported by grant SSI P 476.88 from The National Institute of Radiation Protection and by grants from The Royal Physiographic Society, Lund, The John and Augusta Persson Foundation for Medical Research, Lund, and The Medical Faculty of Lund University.

REFERENCES

1. Loevinger R, Berman M. A revised schema for calculation of the absorbed dose from biologically distributed radionuclides. *MIRD pamphlet no. 1, revised.* New York: Society of Nuclear Medicine; 1976.
2. International Commission on Radiation Units and Measurements. ICRU report 32. *Methods of assessment of absorbed dose in clinical use of radionuclides.* Washington, DC: ICRU; 1979.
3. The International Commission on Radiological protection. ICRP publication 53. *Radiation dose to patients from radiopharmaceuticals.* Oxford, England: Pergamon Press; 1987.
4. Ullberg S. Studies on the distribution and fate of ^{35}S-labeled benzylpenicillin in the body. *Acta Radiol* 1954;(suppl. 118):1–110.
5. Yonekura Y, Brill AB, Som P, Bennett GW, Fand I. Quantitative autoradiography with radiopharmaceuticals, part 1: digital film-analysis system by videodensitometry: concise communication. *J Nucl Med* 1983;24:231–237.
6. Som P, Yonekura Y, Oster ZH, et al. Quantitative autoradiography with radiopharmaceuticals, part 2: applications in radiopharmaceutical research: concise communication. *J Nucl Med* 1983;24:238–244.
7. d'Argy R, Sperber GO, Larsson BS, Ullberg S. Computer-assisted quantification and image processing of whole-body autoradiograms. *J Pharmacol Meth* 1990;24:165–181.
8. Hosain F, McIntyre P, Poulose K, Stern HS, Wagner HN. Binding of trace amounts of ionic indium to plasma transferrin. *Biochem Biophys Acta* 1969;127:66–71.
9. The International Commission on Radiological Protection. ICRP 30. Part 2. *Limits for intakes of radionuclides by workers.* Oxford, England: Pergamon Press; 1980.
10. Beamish MR, Brown B. The metabolism of transferrin-bound ^{111}In and ^{59}Fe in the rat. *Blood* 1974;43:693–701.
11. Desai AG, Thakur ML. Radiolabeled blood cells: techniques and applications. *CRC Critical Rev Clin Lab Sci* 1986;24:95–122.
12. Hinkle GH, Loesch JA, Hill TL, Lefevre SR, Olsen JO. Indium-111-monoclonal antibodies in radioimmunoscintigraphy. *J Nucl Med Technol* 1990;18:16–28.
13. Lamki LM, Patt YZ, Murray JL. In-111 monoclonal antibody immunoscintigraphy of colorectal cancer. In: Goldenberg DM, ed. *Cancer imaging with radiolabeled antibodies.* Norwell, MA: Kluwer Academic Publishers; 1990:293–312.
14. Thakur ML, Thiagarajan P, White III F, Park CH, Maurer PH. Monoclonal antibodies for specific cell labeling: considerations, preparations and preliminary evaluation. *Nucl Med Biol* 1987;51–58:1987.
15. Goodwin DA, Goode R, Brown L, Imborne CJ. Indium-111-labeled transferrin for the detection of tumors. *Radiology* 1971;100:175–179.
16. Farrer PA, Saha GB, Shibita HN. Evaluation of ^{111}In-transferrin as a tumor scanning agent in humans. *J Nucl Med* 1972;13:429.
17. Lillien DL, Berger HG, Anderson DP, Bennett LR. Indium-111-chloride: a new agent for bone marrow imaging. *J Nucl Med* 1973;14:184–186.
18. Gilbert EH, Earle JD, Goris ML, Kaplan HS, Kriss JP. The accuracy of ^{111}In-Cl_3 as a bone marrow scanning agent. *Radiology* 1976;119:167–168.
19. Pauwels EKJ, te Velde J, Hermans J, Haak HL, Jürgens PJ. Indium-111-chloride bone marrow scintigraphy in aplastic anaemia. *Scand J Haematol* 1981;26:81–90.
20. Segal AW, Deteix P, Garcia R, Tooth P, Zanelli P, Allison AC. Indium-111 labeling of leukocytes: a detrimental effect on neutrophil and lymphocyte function and an improved method of cell labeling. *J Nucl Med* 1978;19:1238–1244.
21. Rao DV, Sastry KSR, Grimmond HE, et al. Cytotoxicity of some indium radiopharmaceuticals in mouse testes. *J Nucl Med* 1988;29:375–384.
22. Jönsson BA, Strand SE. Absorbed doses of ^{111}In and ^{114m}In after administration of ^{111}In-complexes with different biokinetics. *Eur J Nucl Med* 1992:submitted.
23. Jönsson B-A, Strand S-E, Andersson L. Biodistribution and absorbed doses of ^{111}In-labeled F(ab')$_2$ fragments in rats. *J Nucl Med* 1992;33:1154–1160.
24. Jönsson BA, Strand SE. Biokinetics and tissue uptake of indium-111 radiopharmaceuticals evaluated in the rat: approaching radiation dosimetry at the cellular level [Abstract]. *Eur J Nucl Med* (suppl). 1990;16:S160.
25. Thörne J, Olsson PI, Strand SE, Jönsson BA, Norgren L. An experimental method for in vivo studies of pulmonary platelet sequestration. *Eur J Nucl Med* 1984;9:472–477.
26. Rövekamp MH, Hardeman MR, van der Schoot JB, Belfer AJ. Indium-111-labelled leukocyte scintigraphy in the diagnosis of inflammatory disease—first results. *Br J Surg* 1981;68:150–153.
27. Weber DA, Eckerman KF, Dillman LT, Ryman JC. *MIRD: radionuclide data and decay schemes.* New York: Society of Nuclear Medicine; 1989.
28. Larsson B, Ullberg S. Whole-body autoradiography. *J Histochem Cytochem* 1981;29:216–225.
29. Ullberg S, Larsson B, Tjävle H. Autoradiography. In: Glenn HJ, Colombetti LG, eds. *Biological applications of radiotracers.* Boca Raton, FL: CRC Press; 1982:55–108.
30. d'Argy R. Short-lived radionuclides and image analysis in whole-body autoradiography [Doctoral thesis]. Uppsala University, Sweden, 1988.
31. Ewans RW, Ogwang W. Interaction of indium with transferrin. *Biochem Soc Trans* 1988;16:833–843.
32. Yeh SM, Meares CF, Goodwin DA. Decomposition rates of radiopharmaceutical indium chelates in serum. *J Radioanalyt Chem* 1979;53:327–336.
33. Cole WC, Denardo SJ, Meares CF, et al. Comparative serum stability of radiochelates for antibody radiopharmaceuticals. *J Nucl Med* 1987;28:83–90.
34. Gatter KC, Brown G, Trowbridge IS, Woolston RE, Mason DY. Transferrin receptors in human tissues: their distribution and possible clinical relevance. *J Clin Pathol* 1983;36:539–545.
35. Huebers HA, Finch CA. The physiology of transferrin and transferrin receptors. *Phys Rev* 1987;67:520–582.
36. Weiner R. The role of transferrin and other receptors in the mechanism of Ga-67 localization. *Nucl Med Biol* 1990;17:141–149.
37. Octave JN, Schneider YJ, Trouet A, Crichton RR. Iron uptake and utilization by mammalian cells. I: cellular uptake of transferrin and iron. *Trend Biochem Sci (TIBS)* 1983;8:217–220.
38. May WS, Cuatrecasas P. Transferrin receptor: Its biological significance. *J Membrane Biol* 1985;88:205–215.
39. Makrigiorgos M, Adelstein SJ, Kassis AI. Limitations of conventional internal dosimetry at the cellular level. *J Nucl Med* 1989;30:1856–1864.
40. Howell RW, Rao DV, Sastry KSR. Macroscopic dosimetry for radioimmunotherapy: nonuniform activity distributions in solid tumors. *Med Phys* 1989;16:66–74.
41. Sgouros G, Barest G, Thekkumthala J, et al. Treatment planning for internal radionuclide therapy: Three-dimensional dosimetry for nonuniformly distributed radionuclides. *J Nucl Med* 1990;31:1884–1891.
42. Roberson PL, Buchsbaum DJ, Heidorn DB, ten Haken RK. Three-dimen-

sional dose-rate distributions for monoclonal antibody treatment: implications for the development of time-integral dose distributions [Abstract]. *Radiat Res* 1991;270:P19:04.
43. Wessels BW, Griffith MH. Miniature thermoluminescent dosimeter absorbed dose measurements in tumor phantom. *J Nucl Med* 1986;27:1308–1314.
44. Griffith MH, Yorke ED, Wessels BW, DeNardo GL, Neacy WP. Direct dose confirmation of quantitative autoradiography with micro-TLD measurements for radioimmunotherapy. *J Nucl Med* 1988;29:1795–1809.
45. Jönsson B-A, Strand S-E, Emanuelsson H, Larsson B. Tissue, cellular, and subcellular distribution of indium radionuclides in the rat. In: Howell RW, Narra VR, Sastry KSR, Rao DV, eds. *Biophysical aspects of Auger processes.* AAPM Symposium Series No. 8. 1992;273–289.
46. Jönsson B-A, Emanuelsson H, Strand S-E. Autoradiographic demonstration of the biodistribution in rat testes of intravenously administered indium. *Radiat Res* 1992:in press.

EDITORIAL

Quantitative Autoradiography for the Study of Radiopharmaceutical Uptake and Dose Heterogeneity

The calculation of absorbed dose estimates is standard practice to help assess risk of injury or probability of therapeutic efficacy in the diagnostic and therapeutic use of radiopharmaceuticals. Even though tissues vary, the response of a single tissue type to a uniform absorbed dose delivered under identical conditions is highly correlated with dose magnitude. The Medical Internal Radiation Dose (MIRD) Committee has developed a methodology for calculating organ doses (*1*) which is often used to calculate "average" doses using the simplified assumptions of uniform activity density and homogeneous organ composition, known as the uniform isotropic model. Use of this simplified model is widespread. However, due primarily to the observed heterogeneity of radiopharmaceutical uptake in tissues (*2–5*), there is growing evidence of its inadequacy.

If the average dose calculations were a valid predictor of effect, there should be a simple relationship between external beam irradiation (XRT) and radioimmunotherapy (RIT). A recent review of XRT/RIT comparisons (*6*) listed relative efficiencies of tumor growth delay to range between 0.3 and 3.3. Possible reasons noted for a decreased efficiency of RIT relative to external beam were: (1) dose rate effect (*7*); and (2) dose heterogeneity. Possible reasons for an increased efficiency were: (1) enhanced reoxygenation with RIT; (2) RIT preferentially targeting rapidly proliferating cells; (3) cell cycle redistribution with accumulation in the radiosensitive G2 phase; (4) cell geometric effect (*8*); and (5) RIT contribution to increased tumor vascular permeability. This illustrates the current uncertainties in the use of calculated dose values using the uniform isotropic model: there appears to be a very tenuous relationship between average dose and outcome with many potential correction factors of uncertain magnitude.

The general MIRD committed methodology does allow for the use of nonuniform activity distributions in source regions and nonuniform size and density of target regions (*1*). However, the greatest obstacle for the use of more realistic models is the collection of accurate input data. A recent editorial (*9*) on the MIRD approach recommends the use of improved measurement techniques for the determination of activity density values at both the cellular and multi-cellular levels for the study of the dosimetric consequences of nonuniform activity distributions. The time variations of the activity distributions can also be significant (*5*). The MIRD methodology includes provisions for the time dependence; but, again, the calculation of a dose distribution for a time-dependent inhomogeneous activity distribution requires a substantial quantity of input data.

Quantitative autoradiography (QAR) can be used to determine the activity density distributions for the whole body, individual organs and tumors. The film optical density scale is calibrated using standards of known activity density, allowing the calculation of activity densities from the autoradiograph data. The quality of the autoradiograph is dependent on the type of film and the type of emitted radiation. The autoradiograph film is typically digitized using an imaging system or optical densitometer. The spatial resolution of the autoradiograph and the pixel size of the digitizer are important parameters. The need for high spatial resolution is dictated by the penetrating ability of the emitted radiation. The digitizer pixel size should be small compared to the distance of significant gradient of the optical density distribution due to its logarithmic dependence on relative light intensity (*10*). Very short range radiations (e.g., Auger emitters or alpha particles) require activity information at the cellular level (<10 μm) (*11*) as input for microdosimetry calculations. For longer range particles, calculations averaged over many cells (~100 μm) is adequate (multicellular dosimetry (*12*)). To obtain the required resolution, the range of the radiations used to produce the autoradiograph must be at least as short as the range of the radiations for which calculations are being performed. The use of low-energy, short-range sources for QAR requires special calibration procedures (*13*).

In this issue of *JNM*, Jonsson et al. (*14*) use whole-body quantitative macro-autoradiography (WBQAR) to study the distribution of uptake in rats

Received Jun. 18, 1992; accepted Jun. 19, 1992.
For reprints contact: Peter L. Roberson, Department of Radiation Oncology, University of Michigan Medical School, Ann Arbor, MI.